Image Analysis of the Atomization Process in a Molten Metal Close-Coupled Atomizer for Different Gas Pressures and Temperatures

Alexander Ariyoshi Zerwas*[1], Kerstin Avila[2,3], José Luís de Paiva [1], Roberto Guardani [1], Lydia Achelis[3], Udo Fritsching [2,3]

[1] Chemical Engineering Department, University of São Paulo, São Paulo, Brazil

[2] Leibniz Institute for Materials Engineering IWT, Badgasteiner Straße 3, 28359 Bremen, Germany

[3] University of Bremen, Faculty of Production Engineering, Particles and Process Engineering, Badgasteiner Straße 1, 28359 Bremen, Germany

*Corresponding author email: alexander.zerwas@usp.br

Abstract

Sprays of molten metal are known to exhibit rich spatio-temporal dynamics, such as a pulsating metal mass flux, or a precession motion of the melt plume. Powerful tools for their investigation are high-speed recordings combined with digital image processing. In this work, we present a method to generate spatio-temporal diagrams from the recordings. These diagrams are ideally suited to quantify spray fluctuations in space and time. Experiments were conducted in an annular close-coupled atomizer using a copper alloy ($CuSn_6$) as base material with varying atomization gas pressures ([0.8, 1.2, 1.6, 2.0] MPa) and temperatures ([293, 423, 523] K). The region of the primary atomization was monitored with a high-speed camera recording 21,800 frames per second. At the parameters investigated we observe an oscillation of the spray boundaries below 100 Hz indicating a slow precession motion. The analysis of the statistically steady spray shape surprisingly reveals a breakdown of the axial symmetry at large gas pressures, whose origin is currently unknown.

Keywords
Primary Atomization, Metal Powder, Multiphase Flow, Image analysis.

Introduction

Additive manufacturing enables the production of high complex metal parts with tailored material gradients, internal channel shapes and geometries, which cannot be produced with traditional manufacturing methods (subtracting processes). Metal powders are the raw material of additive manufacturing and their demand in quantity and quality is increasing rapidly [1]. Metal powders are commonly processed through the atomization of a molten metal jet by a high-speed inert gas jet.

The atomization process is dominated by the interaction of the liquid metal with the high-speed gas stream, which leads to the formation of ligaments and droplets. In close-coupled atomizers as used in this study the interaction occurs close to the nozzle [2]. The atomization regimes in coaxial jets (consisting of a liquid core and an annular gas jet) are typically displayed in phase diagrams. For a liquid of density ρ_l, dynamic viscosity μ_l and surface tension σ exiting a nozzle of diameter L_l with a mean velocity U_l, the relevant dimensionless numbers are the Reynolds ($Re_l = \rho_l U_l L/\mu_l$), Weber ($We_l = \rho_l U_l L_l/\sigma$) and Ohnesorge ($Oh = \sqrt{We}/Re$) numbers [3]. For high gas velocities U_g, another parameter is required to account for the momentum flux ratio ($M = \rho_g {U_g}^2/\rho_l {U_l}^2$) between the liquid and the gas of density ρ_g [4]. The core length of the jet in the primary region (as defined in [5]) depends on the geometry of the atomizer. More specifically it is proportional to the ratios of the exit areas of the liquid and the gas (A_l/A_g) [6, 7].

The atomization of liquid metal is more complex than for ordinary liquids and is influenced by additional parameters, such as the gas properties and the overheat (temperature difference above the alloy liquidus point), which are well-known to influence droplet size distribution [16]. Recently, it has been recognized that the gas temperature also affects the droplet size distribution [17, 18]. For molten metal, two main breakup scenarios are described in literature. In the first one, called melt sheet breakup [8], the molten metal propagates to the boundaries of the gas jet where it is atomized as a sheet. The second one, termed fountain mode [9], is characterized by a build-up of liquid near the nozzle exit, which stems from recirculated liquid, which breaks down.

The analysis of dominating frequencies in the spray is relevant because these are related to the powder size distributions [14]. Oscillations during jet breakup can be analysed with high-speed recording. One example is to divide the field of view in sections and to monitor the amount of liquid in each window over time, from which the oscillation frequencies can be determined [10]. In other studies, a pulsatile motion was observed at low frequencies (<25 Hz) and a precession motion at a higher frequency [11], even for atomization pressures well below the transition between open-wake and close-wake [12]. The precession motion seems to be a rather robust feature of metal molten sprays, as it was also observed for different geometries of the delivery nozzle [13]. In that study, the excited frequencies of a flat tip profile seem to be distributed more uniformly (between 50 and 1500 Hz), compared to the frequencies of other nozzle geometries. Besides the precession motion, there was also an oscillation of the liquid metal mass flux reported that depended on the atomization pressure [12, 25].

We summarize that the atomization of molten metal is a highly complex process and that image processing is a powerful tool to characterize sprays. We here introduce a method to produce spatio-temporal diagrams from high-speed recording. The spatio-temporal diagrams are ideally suited for a statistical analysis of the spray boundaries, including a determination of dominant frequencies, and an identification of the spatial spray asymmetries. We apply this technique to evaluate the atomization of a close-coupled atomizer [19, 24] with a copper alloy (copper with 6%-wt. tin) as liquid and argon as gas (at varying temperatures and pressures).

Materials and Methods

The molten metal atomization experiments were performed in an annular close-coupled atomizer [19], in which the high-speed gas jet (argon) exits through a convergent-divergent nozzle in the vicinity of the liquid jet (1.5 mm diameter), as shown in Error! Reference source not found..

The relation of area ratios between gas nozzle exit and throat is 1.375. Based on a one-dimensional compressible isentropic flow formulation [27] and the reservoir conditions being given inside the atomizer manifold, we estimate that the gas exit velocity U_g was supersonic (between 400 and 560 m/s). The ratio of the atomizer areas is A_l/A_g = 0.034. The setup consisted of two separate chambers. The top chamber is used to heat the metal inside a graphite crucible above the liquidus temperature, and the bottom chamber is used to atomize and collect the powder (after it passes through a small cyclone). An overheat temperature of 350 K was used in all experiments.

Three gas temperatures (cold - 293 K, heated - 423 K, strongly heated - 573 K) and four gas pressures (0.8, 1.2, 1.6, 2.0 MPa) were used. The gas temperature was measured with a thermocouple and the gas pressure with a pressure sensor, both located inside the manifold of the gas nozzle (upstream of the convergent-divergent section). During each experimental run the temperature was set at the beginning and kept fixed, while the gas pressure was varied in between the four values. At each pressure value, a high-speed recording of the spray was taken for 0.45 seconds (starting at least 15 seconds after changing the pressure, to discard

transients). The experiments with the heated gas required a thermal stabilization of the system prior to the measurements. This was achieved by heating the inert gas inside a reservoir and circulating it throughout the setup until the temperature reached the desired value. Only then the liquid atomization was started. In these measurements, the gas temperature increased during atomization up to 30 K due to a higher heated gas temperature.

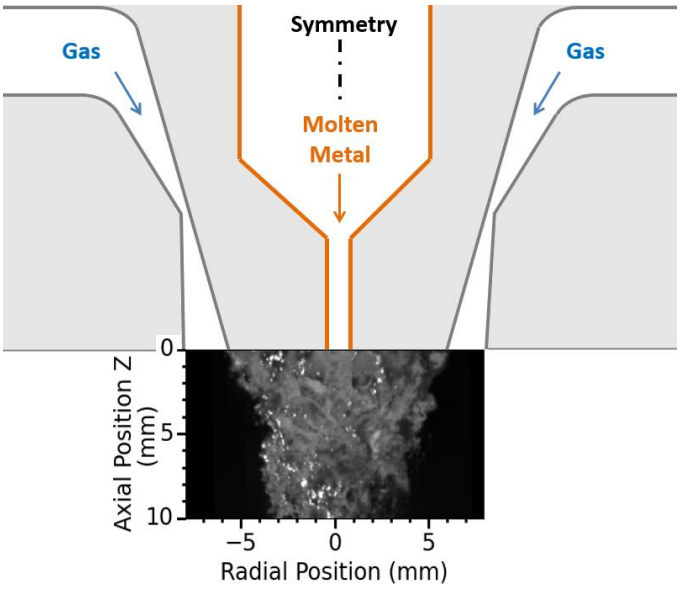

Figure 1. Schematic of the annular close-coupled nozzle (sketch not in scale). The flow of the liquid metal ($CuSn_6$) descents through a straight tube (diameter L_l = 1.5 mm). The flow of argon gas is accelerated through a convergent-divergent nozzle (exit length L_g= 1.1 mm)

In order to analyse the spray in the region where the liquid interacts with the gas, a high-speed camera (Photron – Fastcam SA4 – Type 500K – M1), with an image acquisition speed of 21,800 frames per second (fps) and a pixel resolution of 512x256, was mounted in front of an inspection window at the bottom chamber. Illumination was provided in an angle of 90º to the camera by an intense focalized light source (Dedolight 400D – 400W). Note that the camera was positioned at an angle with the perpendicular plane to the metal jet, which required a camera calibration (described in the next paragraph).

Results and Discussion

Camera calibration

In order to achieve an adequate 3D scale representation of the information contained in the 2D images, a calibration step was needed [20, 21]. Intrinsic parameters (such as the used lenses and their position relative to the camera sensor) as well as extrinsic parameters, which depend on the camera position relative to the object, were evaluated. For the intrinsic parameter estimation an algorithm developed in [22] was used. The calibration plate consisted of a 7x7 checkerboard pattern, which was placed in a focal distance similar to the one of the molten metal spray (approximately 0.5 m). The calibration plate was recorded 39 times at different angles and locations across the field of view of the camera. The corner positions of the checkerboard pattern were evaluated by the algorithm and used in an optimization step to determine the intrinsic camera parameters [22]. The total error was less than 0.51%, which implies that the calibration was done successfully. However, due to the position of the camera, a correction of the perspective distortion (extrinsic parameter) was required. This was done

by placing an affine transformation of the pattern perpendicularly to the nozzle exit surface and using the undistorted pattern image to correct the atomization images. The maximum difference observed was 1.5%.

Generation of spatio-temporal diagrams

A typical snapshot of the molten metal spray as recorded with the high-speed camera is shown in Figure 2a. Bright regions correspond to dense regions of liquid metal, whereas in darker regions the gas dominates. Radial profiles of the light intensity at selected axial positions (see b-e) allow therefore an estimative of the width of the spray core and its spatial fluctuations. To include also temporal fluctuations in our analysis, we extract from each snapshot the radial profiles of the light intensity at 16 axial positions (four of the positions are indicated by the red lines in Figure 2a) and plot them over time. This procedure generates a spatio-temporal diagram (as shown in Figure 3) at each axial position. More details of this method are provided in [23].

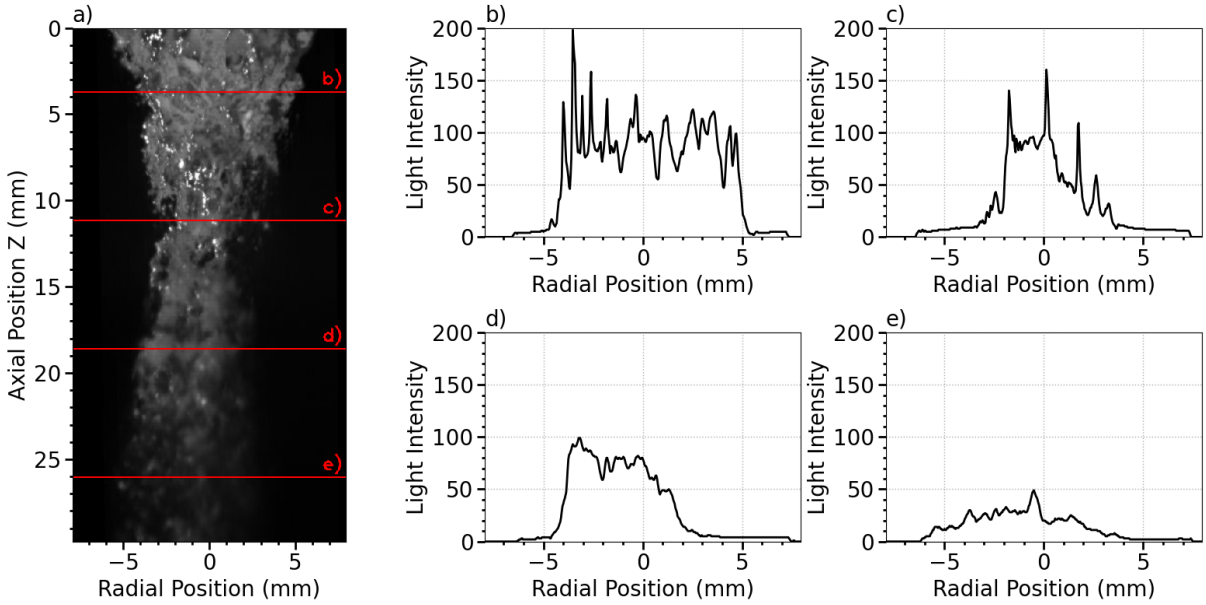

Figure 2. Typical snapshot of the high-speed recording illustrating the molten metal spray. The flow was evaluated at 16 axial positions beneath the nozzle exit (Z = 0 mm). Light intensity profiles at four selected positions, marked by the red lines at Z = 3.7 mm (b), Z = 11 mm (c), Z = 18.5 mm (d), Z = 25.8 mm (e), show the variations in space.

Analyses of the spatio-temporal dynamics

A typical spatio-temporal diagram of the flow is shown in Figure **3** for a time interval of 0.05s (corresponding to about 10% of the total measurement time). Bright regions correspond again to liquid metal and dark regions to the gas. A threshold in light intensity was used to determine the borders of the liquid core (indicated by the blue and green line). The threshold was adopted as the mean value between the maximal light intensity and the value obtained in a liquid-free region (e.g. close to the image border). The instantaneous geometrical mean position of the spray (shown as a red line), and its instantaneous width, can be easily calculated from the spray boundaries (shown as green and blue lines). In the observed time, the fluctuations of the right spray border (indicated by the blue line) are very strong and have a periodicity (of about 0.006s) well below the high-frequency fluctuations. A more detailed analysis of the dominant frequencies (obtained with a Fast Fourier Transformation, FFT) leads to the

frequency spectra shown in Figure 4. Indeed, the spectrum of the right spray border shown in a) confirms a frequency peak at 150Hz, which corresponds to the oscillation with a periodicity of 0.006s already visible in the spatio-temporal diagram. However, the dominant mode has an even lower frequency (of about 40 Hz) and dominates also in the left spray border (see **b)**), and therefore also in the spray position (see **c)**). By contrast, the spectrum of the spray width shown in **d)** does not exhibit a high-amplitude oscillation at 40 Hz, which indicates that the low-frequency oscillation of the borders may stem from a precession motion. In the literature, precession motions have been observed directly beneath the nozzle and with similar frequencies [14, 15]. Fluctuations were mainly below 200 Hz in all axial positions.

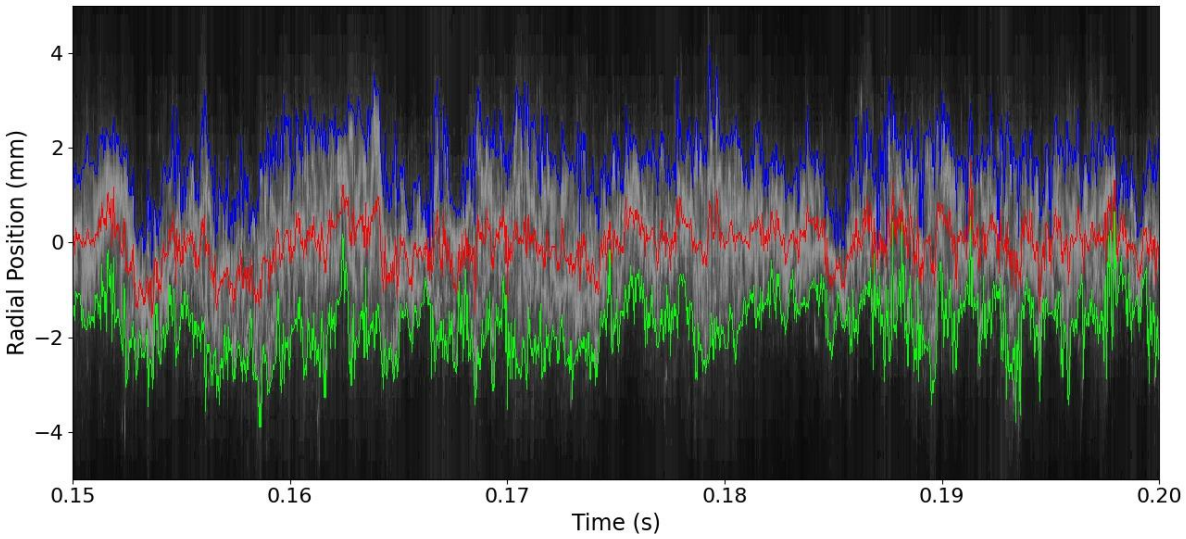

Figure 3. Spatio-temporal diagram (at axial position z = 20.4mm) generated from high-speed video recordings of the atomization area. The spray boundaries in the radial direction, identified from the image processing, are indicated by the blue and the green line (corresponding to the right and left boundary of the spray in the original images). In this measurement, the atomization was performed at a gas temperature of 423 K and a gas pressure of 1.2 MPa. About 10% of the total measurement time is shown.

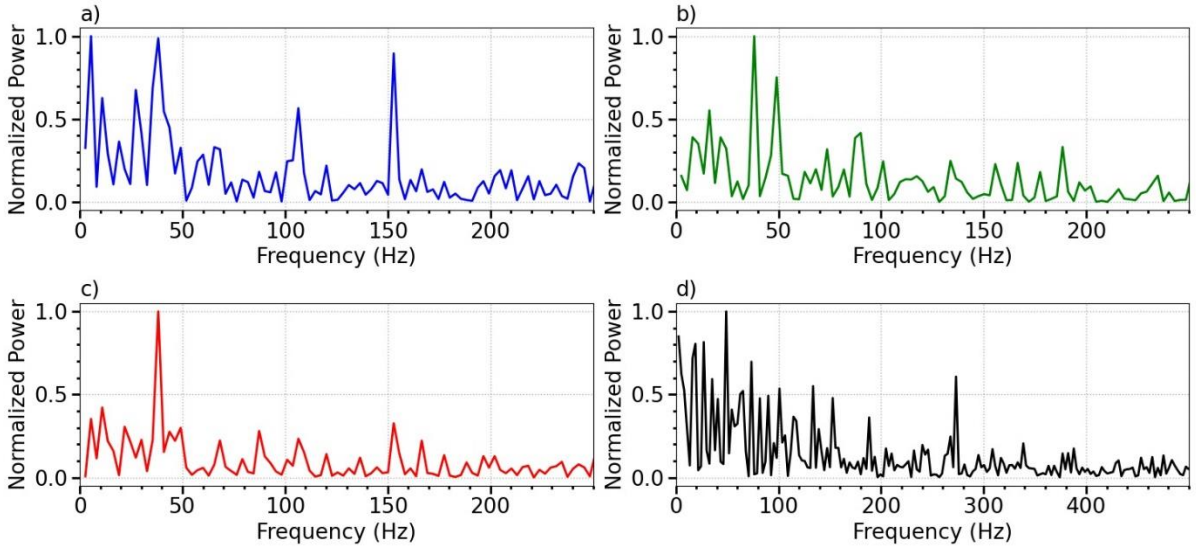

Figure 4. Normalized power spectrum of the radial positions of the spray boundaries (in a) and b)), the geometric mean position (c)) and mean width (d). The power spectra are obtained from the image processing of the spatio-temporal diagram, partly shown in Figure 3.

Compared to the position of the spray boundaries, the width of the spray has a broader frequency spectrum with less distinct peaks. An increase of the gas pressure seems to first enhance higher frequencies as it is displayed in **Figure 5a**, before a further increase causes again an excitation of the lower oscillation frequencies as illustrated in **b)**. In order to understand the mechanisms behind these observations, their reproducibility should first be tested by repeating the measurements several times. This would allow it to distinguish between fluctuations occurring at identical process conditions and the ones characteristic for an increase of the gas pressure.

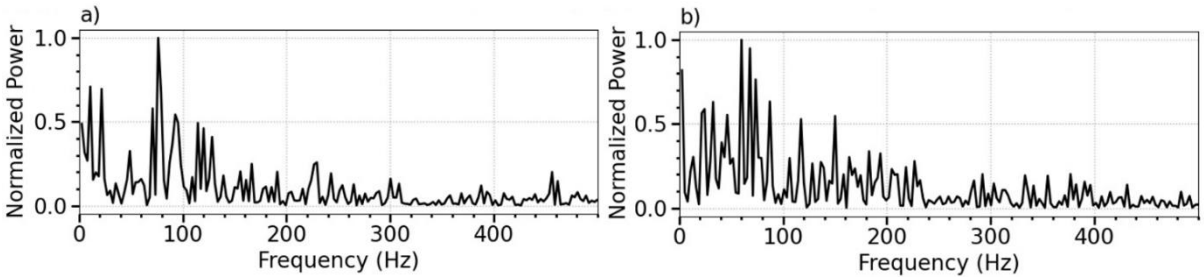

Figure 5. Normalized power spectrum of the spray width for a gas temperature of 423 K and a gas pressure of 1.6 MPa in a) and 2.0 MPa in b). The spectrum was determined at an axial position z = 20.4 mm.

Statistical analysis of the spray shape

In the previous section the temporal behaviour of the spray boundaries and the spray width were analysed. In this section we focus on the spatial aspects of the dynamics. From a single spatio-temporal diagram, we retrieve the mean position (averaged over time) and the standard deviation of both spray boundaries. This procedure is applied to all the 16 space-time diagrams at varying axial positions. The results of these analyses are shown in **Figure 6a)** and represent the time-averaged spray shape together with its fluctuations in time and space. Directly beneath the nozzle (for z < 6 mm) the width of the spray quickly decreases, as is expected for this type of atomizer. Overall, the mean shape of the spray is surprisingly asymmetric. In this measurement the fluctuations are substantially smaller than the observed asymmetry, which indicates that the spray becomes intrinsically non-axisymmetric below the nozzle. Currently, we cannot distinguish if this asymmetry is caused by e.g. a slightly asymmetric nozzle (due to fabrication uncertainties) or if the spray dynamics itself becomes asymmetric (e.g. because of a symmetry-breaking instability).

The width of the spray core is plotted in **b)** following a continuous decrease in an axial distance from the nozzle z < 10 mm (corresponding to 6.6 L_l, where L_l is the nozzle diameter) before settling to a width of about 1 mm.

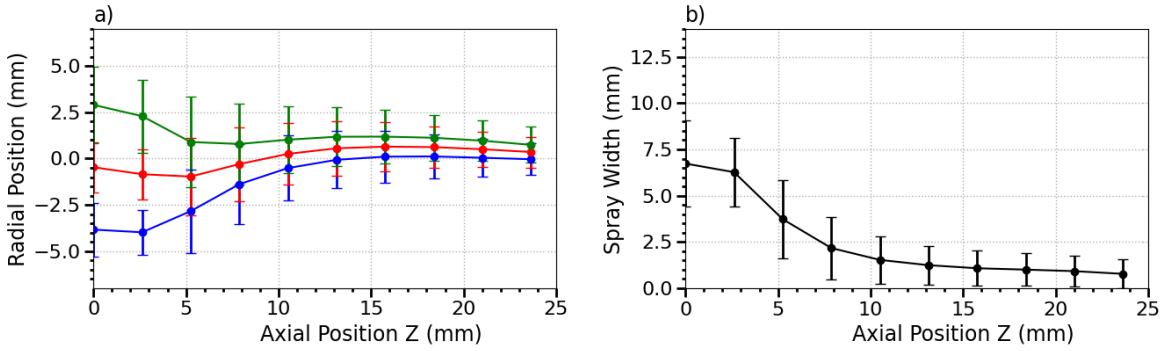

Figure 6. Statistically obtained spray shape (at a gas temperature of 573 K and a gas pressure of 2.0 MPa). Each data point corresponds to the time-averaged value of a selected spray property gained from a spatio-temporal diagram at an axial position Z. The measured standard deviation in time is represented by vertical bars. a) Time-averaged spray boundaries are indicated by the blue and green symbols; the red symbols denote the geometric mean position. An asymmetric shape is clearly visible. b) Time-averaged spray width.

Conclusions

In this study, we investigated experimentally the molten metal atomization of a copper alloy ($CuSn_6$), under different atomization gas pressures (0.8, 1.2, 1.6, 2.0 MPa) and temperatures (293, 423, 523 K) by analysing high-speed recordings.
We introduced a method of generating spatio-temporal diagrams from the recordings that allow it to reliably obtain the mean shape and position of the spray core, and to quantify the fluctuations of liquid detachment in space and time.
The mean position of the spray core (as well as its boundaries) oscillates in the radial direction with a frequency of about 40 Hz (at 1.2 MPa, 423 K), indicating a precession motion. In addition, we surprisingly observe that the mean shape of the spray core is highly asymmetric, for certain parameters. The origin of this asymmetry is currently unknown, more measurements and a refined analysis are required to elucidate the underlying dynamics.
In numerical simulations of sprays the full azimuthal length is rarely computed, but instead the domain is reduced to an angle of e.g. 90° and the spray then assumed to be axisymmetric. Our experiments suggest that this procedure may not always be appropriate.

Acknowledgments

A. A. Zerwas gratefully acknowledges the financial support received from CAPES, by the PhD sandwich program from PrInt-USP for the stay at the University of Bremen and CNPq for the scholarship awarded. K. A. acknowledges support for an `Independent Project for Postdocs' from the Central Research Development Fund of the University of Bremen.

References

[1] Henein, H., Uhlenwinkel, V., Fritsching, U., 2017, "Metal Sprays and Spray Deposition", Springer.
[2] Antipas, G. S. E., 2013, Powder Metallurgy, 56(4), pp. 317-330.
[3] Hopfinger, E. J., Jun. 30.- Jun. 3., 1998, Seventh European Turbulence Conference (Advances in Turbulence VII), pp. 69-78.
[4] Lasheras, J. C., Villermaux, E., Hopfinger, E. J., 1998, Journal of Fluid Mechanics, 357, pp. 351-379.
[5] Leroux B., Delabroy, O., Lacas, F., 2007, Atomization of Sprays, 17, pp. 381-407.

[6] Zhao, H., Liu, H.-F., Tian, X.-S., Xu, J.-L., Li, W.-F., Lin, K.-F., Transport Phenomena and Fluid Mechanics, 2014, 60(6), pp. 2335-2345.
[7] Shumaker, S. A., Danczyk, S. A., Lightfoot, M. D. A., Kastergren, A. L., Jul. 28.-30. 2014, 50th Joint Propulsion Conference.
[8] Ünal, A., 1989, Metalurgical Transactions B, 20, pp. 61-69.
[9] Mates, S. P., Settles, G. S., 2005, Atomization and Sprays, 15, pp. 41-59.
[10] Ting, J., Connor, J., Ridder, S., 2005, Materials Science and Engineering A., 390, pp. 452-460.
[11] McCarthy, I. N., Adkins, N. J., Aslam, Z., Mullis, A. M., Cochrane, R. F., 2009, Powder Mettalurgy, 52(3), pp. 205-2012.
[12] Ting, J., Peretti, M. W., Eisen, W. B., 2002, Materials Science and Engineering A., 326, pp. 110-121.
[13] Mullis, A. M., McCarthy, I. N., Cochrane, R. F., 2011, Journal of Materials Processing Technology, 2011, pp. 1471-1477.
[14] Anderson, I. E., Rieken, J. R., Meyer, J., Byrd, D., Heidloff, A., May 18.-21. 2011, PowderMet 2011.
[15] Kumar A., Sahu, S., 2020, Chemical Engineering Science, 221.
[16] Ünal, A., 1987, Materials Science and Technology, 3, pp. 1029-1039.
[17] Czisch, C., Fritsching, U., 2008, Materials Science and Engineering A, 477, pp. 21-25.
[18] Ciftci, N., Ellendt, N., Barreto, E. S., Mädler, L., Uhlenwinkel, V., 2018, Advanced Powder Technology, 29, pp. 380-385.
[19] Schwenck, D., Ellendt, N.,Bühner, J. F., Hofmann, P., Uhlenwinkel, V., 2017, Powder Mettalurgy, 60(3), pp. 198-207.
[20] Tsai, R. Y., 1987, IEEE Journal of Robotics and Automation, 3(4), pp. 323-344.
[21] Forsyth, D. A., Ponce, J., 2011, "Computer Vision: A Modern Approach", Pearson.
[22] Zhang, Z., 2000, IEEE Transactions on Pattern Analysis and Machine Intelligence, 22(11), pp. 1330-1334.
[23] Avila, K., Hof, B., 2013, Review of Scientific Instruments, 84.
[24] Hussain, S., Cui, C., He, L., Mädler, L., Uhlenwinkel, V., 2020, Journal of Materials Processing Technology, 282, pp.1-8.
[25] Mullis, A., Adkins, N. J., Aslam, Z., McCarthy, I., Cochrane, R. F., 2008, International Journal of Powder Metallurgy, 44, pp. 55-64.
[26] Drahoš, J., Čermák, J., Guardani, R., Schügerl, K., 1988, Powder Technology, 46, pp. 41-48.
[27] Anderson Jr, J. D., 1991, “Fundamentals of Aerodynamics”, McGrawHill.